Surge-Current capability of the different voltage class IGBTs

[1]M. L. Mysore, [1]M. Alaluss, [1]F. Fraas, [1]J. Lutz, [1]T. Basler, [2]R. Baburske, [2]F.-J. Niedernostheide, [2]H.-J. Schulze

[1]Chemnitz University of Technology, Chair of Power Electronics, Chemnitz, Germany
Tel: +49371 531-36091

[2]Infineon Technologies AG, Neubiberg, Germany

Abstract

In this work, the surge-current capability of 650 V, 1200 V, and 1700 V IGBTs has been investigated. This stress condition is important for the active short-circuit of motor loads. For all measurement conditions, the destruction of the devices is not determined by the onset of intrinsic conductivity. Instead, the failure signature indicates a temperature-driven destruction mechanism. For the applied gate-emitter voltages, the 650 V IGBTs show the highest surge-current density withstand capability in comparison to 1200 V and 1700 V IGBTs due to their higher saturation current density. The surge-current capability of 1200 V and 1700 V IGBTs is not influenced by the amount of emitter bond wires even at a gate-emitter voltage of 25 V, whereas it is reduced for 650 V IGBTs with a reduced number of bond wires.

Keywords: IGBT, surge-current, surge-current capability, robustness, bond wire, Al metallization.

INTRODUCTION

IGBTs are widely used power semiconductor devices in medium and high power switching applications. For many applications, short-circuit is a necessary chip requirement. However, there is typically no specification of a surge-current capability that determines the device's ability to withstand and operate under very high current transients or surges. This requirement is naturally in contradiction to the short-circuit ruggedness. Only in special cases, a surge-current operation of IGBTs is beneficial. It can be used to protect the load from alternating torques due to asymmetric short-circuit failures in IGBT converters as described in [1-4]. The active short-circuit of motor loads is one example of this case. Grid errors such as voltage spikes and overvoltage conditions can generate a surge-current for grid-side connected power semiconductor devices (e.g. PFC/rectifier diodes, rectifying switches).

Previous work has demonstrated that IGBTs can conduct high surge-currents at higher gate-emitter voltages by preventing the collector-emitter voltage (V_{CE}) desaturation [1–6]. The surge-current behaviour for different IGBT designs is discussed in [3,7]. Further details regarding the surge-current theory of bipolar devices can be found in [8–11]. The degradation of the chip solder by ageing has a strong influence on the surge-current capability of the IGBT and has been discussed in [12].

In the present work, single pulse surge-current measurements were performed for different voltage class IGBTs with trench technology using an open chip soldered on a direct copper bonded (DCB) substrate. All the measured IGBTs have a similar assembly and interconnect technology (AIT). The surge-current capability of all the IGBTs was measured at distinct gate-emitter voltages and for varying starting temperatures. Also, the influence of the pulse width on the 1700 V IGBT surge-current capability has been studied.

In power semiconductor devices, such as diodes or IGBTs, the bond wires play a crucial role in carrying electrical current. Hence, the impact of the number of emitter bond wires on the surge-current capability of the different voltage class IGBTs has been investigated in detail.

CURRENT LIMITATION OF THE IGBTS

The saturation current $I_{C,sat}$ of the IGBT limits the surge-current capability. Consequently, the IGBT must be prevented from channel pinch-off and V_{CE} desaturation during surge-current operation. Otherwise, it leads to higher losses and destruction. According to the simple MOSFET model the pinch-off voltage $V_{CE,pinch}$ of the MOS channel with a threshold voltage V_{TH}, is given by

$$V_{\mathrm{CE,pinch}} = V_{\mathrm{GE}} - V_{\mathrm{TH}} \qquad (1)$$

for a given gate-emitter voltage V_{GE}. The output characteristics of the different IGBTs are compared with each other by their normalized saturation collector-current density ($J_{C,sat}$). Each voltage class IGBTs was normalized by choosing the appropriate normalized current. The ratio of $I_{C,sat}$ by its active area of the IGBT chip is plotted as a function of gate-emitter voltages for two different temperatures as shown in Fig.1. As can be

seen for both temperatures, the 650 V IGBT shows the highest $J_{C,sat}$ compared to the other two voltage class IGBTs. The saturation current density of the 1200 V IGBT is only slightly higher than the 1700 V IGBT. For the IGBT saturation mode, $I_{C,sat}$ depends on V_{GE} by a quadratic function:

$$I_{C,sat} = \frac{1}{1-\alpha_{pnp}} \cdot \frac{k}{2}(V_{GE} - V_{TH})^2 \qquad (2)$$

where k is a channel-geometry parameter and α_{pnp} the bipolar current gain of the pnp transistor. The main temperature dependent parameters in Eq. (2) are the threshold voltage $V_{TH,}$ α_{pnp} and the electron mobility μ_n which is included in the parameter k.

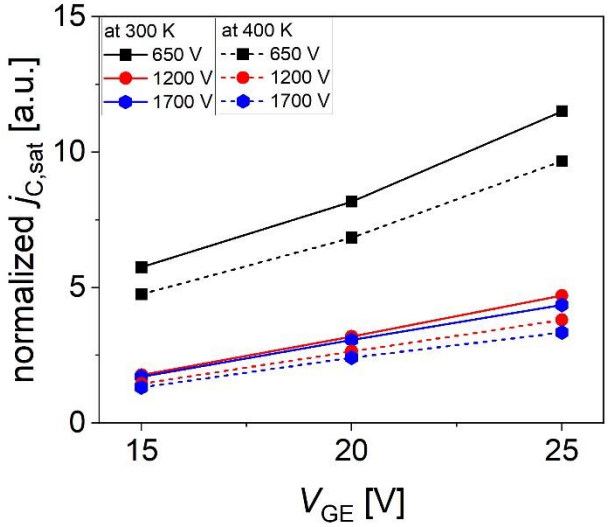

Fig. 1: Normalized saturation collector-current density of the different voltage class IGBTs with varying gate-emitter voltage.

SURGE-CURRENT MEASUREMENT

For investigating the surge-current capability of the IGBTs, a test setup described in [13] was used. During the measurements, a calibration current of 10 mA flowed through the device under test (DUT) IGBT to estimate the junction temperature before and after the surge-current pulse. The junction temperature was estimated using the $V_{CE}(T)$ – method. The V_{CE}(T) calibration curve is predetermined for the different DUTs at different V_{GE} for a temperature range from 295 K to 430 K. The surge-current capability was measured by gradually increasing the surge-current amplitude $\hat{\jmath}_{FSM}$ in steps until a destruction of the DUT occurs or a static electric parameter such as gate-leakage current or $V_{CE,sat}$ or blocking leakage current has changed. Further, the surge-current measurements were carried out at different gate-emitter voltages at varying starting temperatures (T_{start}). Additionally, the influence of the different surge-current pulse-width (t_p) was analyzed for the 1700 V IGBT. For all the surge-current density plots, the normalization was done by choosing the appropriate normalized current density for each voltage class IGBTs.

a) Surge-Current measurements at 10 ms

Initially, the surge-current measurements were carried out with half-sine pulses with t_p of 10 ms, which corresponds to the grid frequency of 50 Hz. The corresponding voltages across the collector and sense-emitter ($V_{CE,sense}$) and across the collector and load-emitter ($V_{CE,load}$) are recorded.

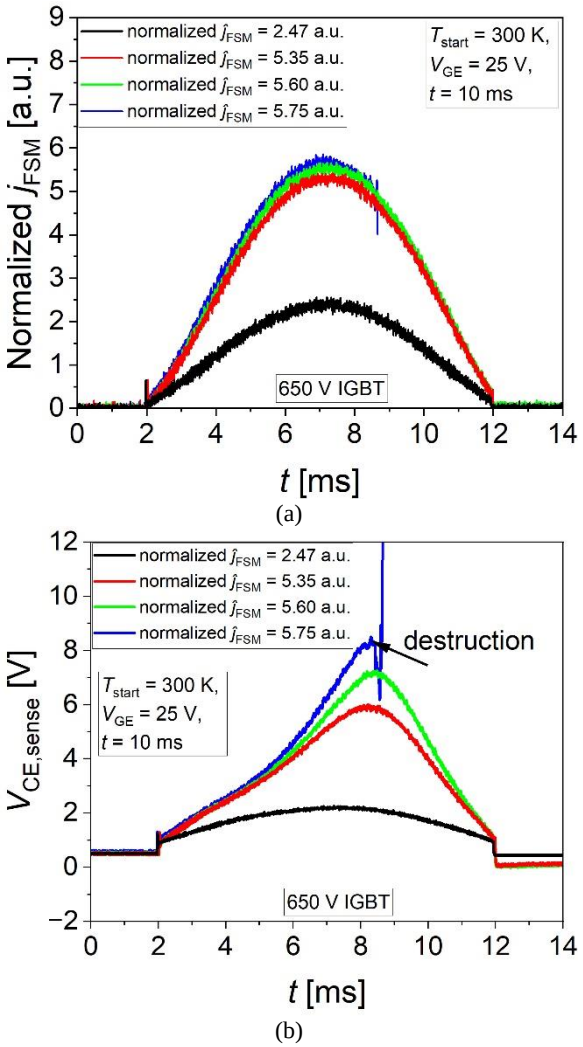

Fig. 2: (a) Measured normalized surge-current capability of the 650 V IGBT increasing the surge-current density amplitude $\hat{\jmath}_{FSM}$ (normalized) (b) measured $V_{CE,sense}$ across the IGBT. For measurement conditions: t_p = 10 ms, V_{GE} = 25 V, T_{start} = 300 K.

For the time interval between 0 ms and 2 ms, before the surge-current is applied [see, Fig. 2(a)], the V_{GE} is set to a high level and the calibration current of 10 mA is flowing. Hence, $V_{CE,sense}$ shows a voltage drop of approximately 0.6 V, which corresponds to the built-in potential of the backside pn-junction at room temperature as shown in Fig. 2(b). As the applied surge-current amplitude is increased across the IGBT, the $V_{CE,sense}$ voltage waveform has its peak after the surge-current

density peak and is strongly deviating from sine-shaped due to the temperature rise in the chip. Applying high currents close to the saturation current leads to a sharp increase in the voltage. After the IGBT has passed the surge-current pulse, the $V_{CE,sense}$ shows a lower voltage drop compared to the starting value, especially at increased surge-current amplitude [Fig. 2(b) after 12 ms] because the built-in potential of the pn-junction is decreased due to significant temperature increase. It is interesting that the falling branches have almost the same V_{CE} at t = 11.75 ms, although the dissipated losses are much different. However, the high V_{GE} compensates for a higher V_{CE}. When the surge-current density amplitude ($\hat{\jmath}_{FSM}$) was increased to 5.75 a.u., the 650 V IGBT failed due to the beginning of V_{CE}-desaturation and correspondingly a higher loss although the V_{GE} value was at 25 V. In contrast to the expected quadratic relation between $I_{C,sat}$ and V_{GE}, see Eq. (1). The measured surge-current capability of the 650 V IGBT at V_{GE} = 25 V and starting temperature of 300 K shows a more linear relation between surge-current and gate voltage. This is due to the self-heating of the device during the surge-current pulse which leads to a lower saturation current of the IGBT. Hence, the n-channel is pinched-off earlier [7]. For the last-pass pulse with $\hat{\jmath}_{FSM}$ of 5.60 a.u., the junction temperature at 12.2 ms is 506 K, estimated via $V_{CE}(T)$ method. It should be noted that the maximum junction temperature will be much higher during the pulse.

For the 1700 V IGBT, the measured last-pass pulse at different gate-emitter voltages at 300 K is shown in $j_{FSM}(V_{CE})$ characteristic in Fig. 3(a). At V_{GE} = 15 V, the MOS channel is pinched off earlier in comparison to V_{GE} of 25 V [Eq. (1) and (2)]. The spread between the rising and falling branches is smaller at V_{GE} = 15 V due to lower dissipated overall losses. However, with higher V_{GE} the thermal hysteresis increases because the IGBT reaches its critical saturation collector-current later and makes less losses from the beginning. The estimated junction temperature is 346 K at 15 V and 512 K at 25 V at t = 12.2 ms, i.e. 0.2 ms after the surge current pulse. At high currents, a positive temperature coefficient (PTC) is observed during the surge-current transient. At the descending branch and the lower currents, a negative temperature coefficient (NTC) is visible mainly from the reduced built-in voltage of the collector-side pn-junction. Furthermore, at such high temperatures, the charge carrier mobilities are strongly reduced. Consequently, the charge carrier concentration in the low doped drift region with a width w_B will change as can be estimated by the following simplified equation for the mean carrier concentrations $\bar{n}$, $\bar{p}$, in the drift region [5]:

$$\bar{n} = \bar{p} = \frac{j \cdot w_B}{V_{drift} \cdot q \cdot (\mu_n + \mu_p)} \qquad (3)$$

where V_{drift} is the voltage drop across the low doped drift region and j is the current density.

The influence of the starting temperature at V_{GE} = 25 V is illustrated in the $j_{FSM}(V_{CE})$ characteristic in Fig. 3(b). At 300 K, the thermal hysteresis between the branches is larger due to higher losses accompanied by the higher applied surge-current compared to 425 K. At the falling branch, the $V_{CE,sense}$ voltages are higher due to the higher starting chip temperature [2]. For the same V_{GE}, the saturation current decreases as the temperature increases, mainly due to reduced mobilities.

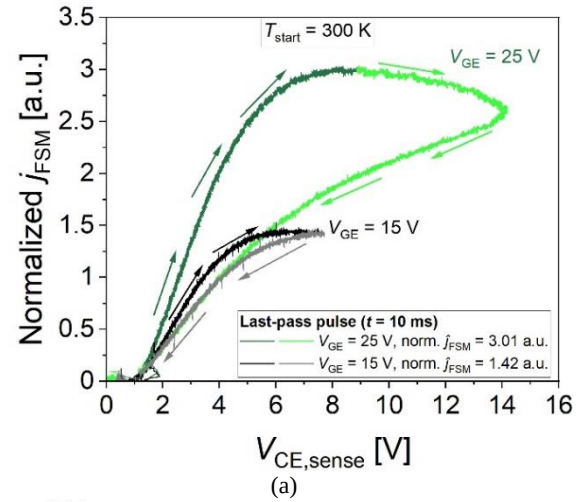

(a)

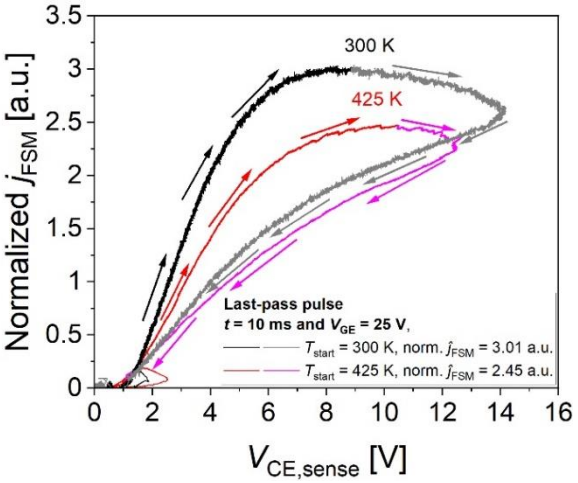

(b)

Fig. 3: Measured last-pass normalized surge-current pulse of 1700 V IGBT (a) for gate-emitter voltages of 15 V and 25 V at T_{start} = 300 K. (b) at different starting temperatures for V_{GE} = 25 V. Conditions: t_p = 10 ms.

The last-pass surge-current and energy density of the different voltage class IGBTs are compared at 300 K and 425 K, in Fig. 4. Two devices each of the 650 V and 1700 V classes and four devices of the 1200 V IGBTs were considered for room temperature measurements. At 425 K, only one device was used in the destructive test, except for the 1200 V class. At V_{GE} = 15 V and at both temperatures, 1200 V IGBTs do not show any failure since the current could not be increased further due to the limitation of the used DC-link capacitors in the test-bench. For both gate voltages and temperatures, the 650 V IGBTs show a higher surge-current density in than the 1200 V and 1700 V IGBTs, which is correlating with the respective nominal current densities of the IGBTs. It

is also visible, that the energy density of all the voltage classes is in the same range for V_{GE} = 25 V.

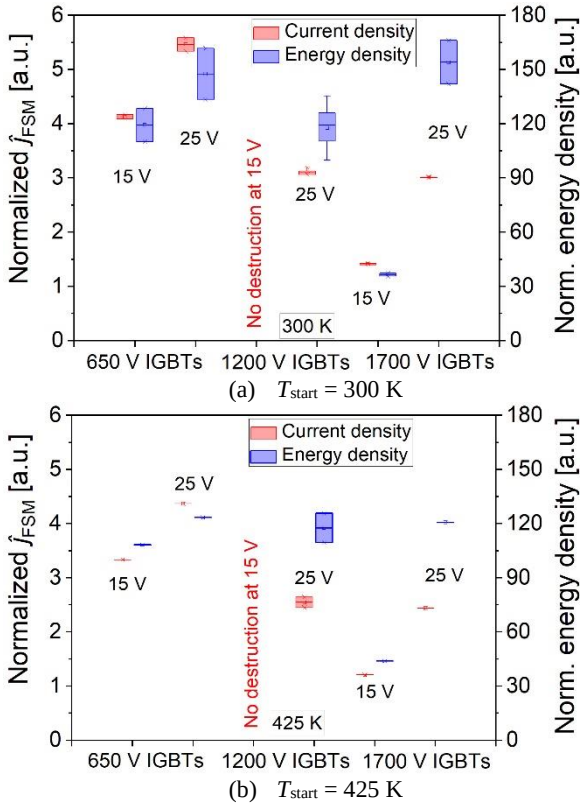

Fig. 4: Comparison of the last-pass maximum normalized surge-current density and corresponding normalized energy density of the different voltage class IGBTs for different gate-emitter voltages at t_p = 10 ms.

For all the measured IGBTs, $V_{CE,sat}$, gate leakage current and collector-emitter leakage current was recorded after each single surge-current event and compared with the initial values measured before. However, there was no drift in any of these analysed parameters.

b) Surge-Current measurements at 1 ms

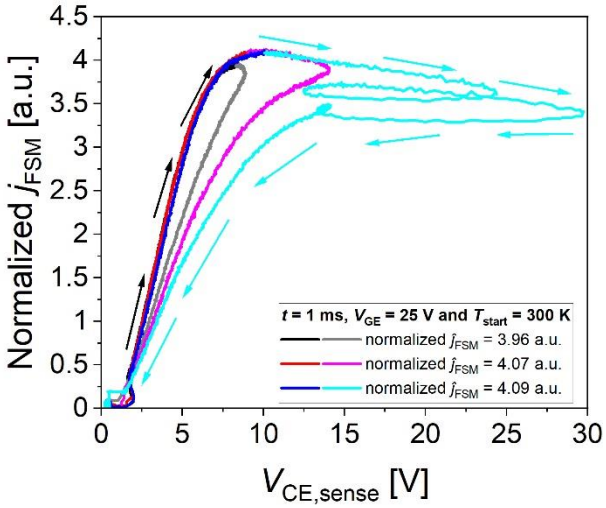

Fig. 5: Measured normalized $j_{FSM}(V_{CE})$ characteristic of a 1700 V IGBT with increased surge-current density at t_p = 1 ms. Conditions: V_{GE} = 25 V, T_{start} = 300 K.

A surge-current can appear in various waveforms depending e.g. on the actual output current frequency of an inverter. Standard tests and datasheet ratings typically use a half-sine wave with a duration between 100 µs and 100 ms [14]. For the results presented here, the surge-current pulse width was set to 1 ms. As shown in Fig. 5, at V_{GE} = 25 V, the 1700 V IGBT reached its saturation collector-current without any failure and a similar behaviour was observed at V_{GE} = 15 V. As the energy dissipation was 10 times lower as compared to 10 ms pulse, the junction temperature was lower as well (307 K at 15 V and 370 K at 25 V). Due to the limited capacitance of the DC-link capacitors in the test-bench further tests at even higher V_{GE} were not carried out.

INFLUENCE OF EMITTER BOND WIRE CONFIGURATION ON SURGE-CURRENT ROBUSTNESS

For all the measured IGBTs, the bond wires are made of aluminium and have a specific cross-sectional area with a diameter of 250 µm that determines their ampacity. During surge conditions, when a high current is flowing through the device, the bond wires will experience an increased current density and high temperatures as a consequence. For high temperatures, the wire resistance increases causing higher voltage drops and power dissipation and describes a positive feedback loop. Further, for a smaller amount of bond wires, the current imprint to the chip's metallization is more inhomogeneous. The typical failure signature for diodes reveals a weak area around the bond wires where the current density and the heat flow is high. Since the Al metallization and the bond wires act as a thermal capacity more bond wires and thicker Al metallization improve the surge-current robustness [11]. Cu metallization and Cu bond wires lead to a further improvement of surge-current ruggedness [15].

To study the influence of a different number of emitter bond wires, 1200 V IGBTs were equipped with 1 emitter bond wire (1EB) and 3 emitter bond wires (3EB) and were compared, see Fig. 6.

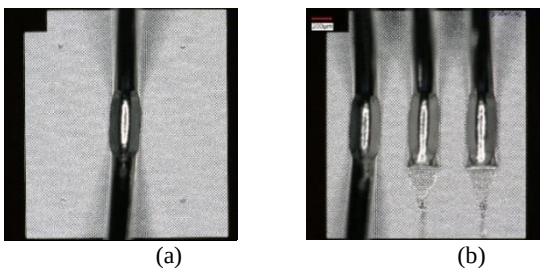

(a) (b)

Fig. 6: 1200 V IGBTs used in surge-current measurements with (a) 1 emitter bond wire (1EB) and (b) 3 emitter bond wires (3EB).

The measured last-pass j_{FSM}-V_{CE} phase space diagram for 1EB and 3EB is shown in Fig. 7(a). The IGBT with 1EB shows a higher voltage drop as compared to the 3EB.

Correspondingly, the energy loss is 9% higher for the 1EB DUT for the same surge-current. With respect to the last-pass current, the surge-current capability of the 1200 V IGBT with 1EB and 3EB is the same as shown in Fig. 7(b), at least for V_{GE} = 25 V. The 1EB chip shows a deep crater within the active area due to a possible bond wire melting and open circuit after surge-current destruction with a subsequent arc, see Fig. 8(a). However, the IGBT with 3EB shows a surface melting of the top-side metallization and the bond wires were not yet lifted or melted, see Fig. 8(b). This is different to the findings on pin-diode structures, where a larger number of bond wires is beneficial. However, the observed failure seems to be more chip related due to the starting desaturation process and high intrinsic IGBT losses and is not yet caused by an overload of the bond wires. Hence, surge-current measurements were performed at higher V_{GE} to study the limiting factor of the bond wires.

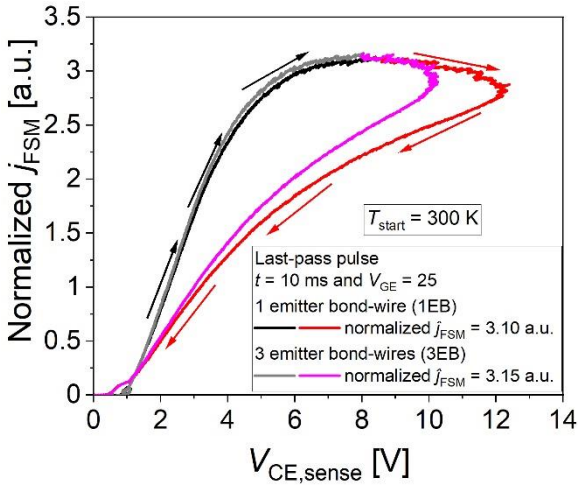

(a)

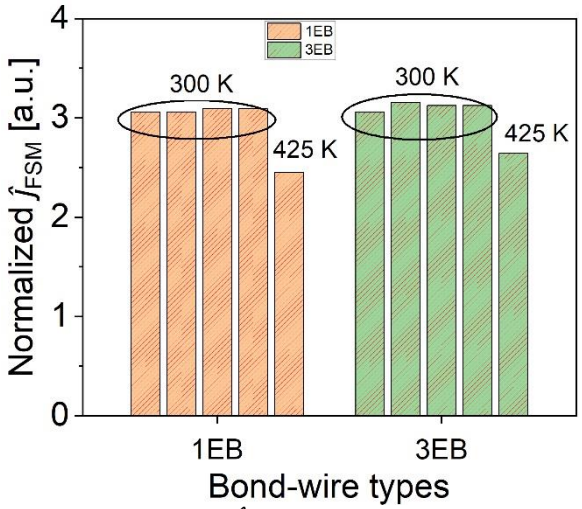

(b) $\hat{J}_{FSM}$ for 1EB and 3EB

Fig. 7: (a) Measured last-pass normalized surge-current $j_{FSM}(V_{CE})$ characteristic of 1200 V IGBT for 1EB and 3EB. (b) Comparison of the 1EB and 3EB last-pass maximum normalized surge-current density of the 1200 V IGBT. For a given condition of t_p = 10 ms, V_{GE} = 25 V and T_{start} = 300 K.

(a) (b)

Fig. 8: Microscopic pictures of the failed IGBT chips during surge-current at V_{GE} = 25 V with (a) 1EB and (b) 3EB.

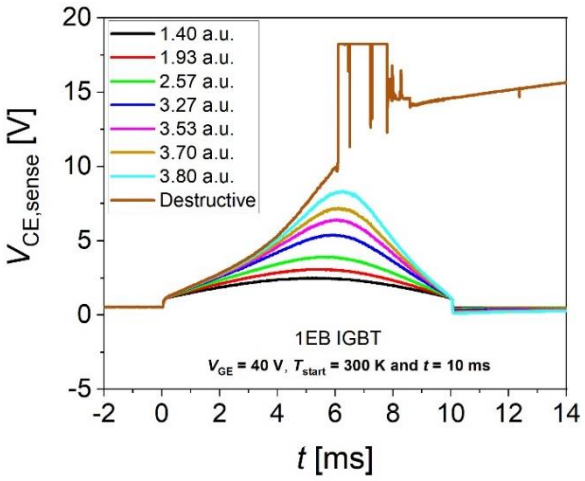

(a)

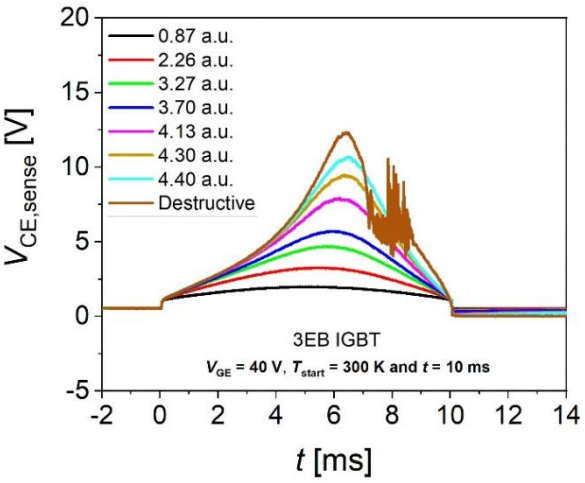

(b)

Fig. 9: Measured $V_{CE,sense}$ across the IGBT for increasing the surge-current density amplitude at V_{GE} = 40 V (a) 1EB (b) 3EB. For a given condition of t_p = 10 ms, and T_{start} = 300 K.

As already indicated above, multiple bond wires provide multiple paths for current flow, which can help to distribute the current more homogeneous across the IGBT. This can result in better heat dissipation and lower localized heating, potentially enhancing the surge-current capability. Thus, the overall current-carrying capacity of the 3EB IGBT is 16% higher at V_{GE} = 40 V as compared to 1EB IGBT, see Figures 9(a) and 9(b). During the destructive pulse, $V_{CE,sense}$ exceeds the measurement range as shown in Fig. 9(a). Here, both IGBTs fail as soon as the devices enter the current saturation regime

[7]. The failure signatures at V_{GE} = 40 V shown in Fig. 10 for 1EB and 3EB are similar to the Fig. 8. The last-pass surge-current of the 1200 V IGBTs for 1EB and 3EB at different V_{GE} are compared in Table 1.

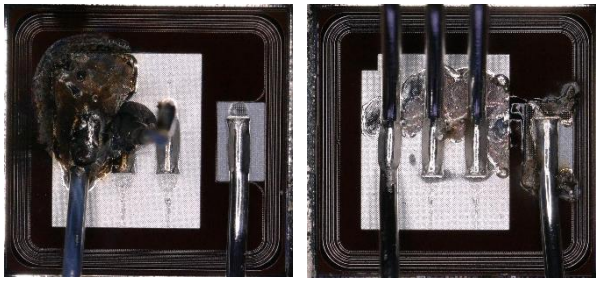

(a) (b)

Fig. 10: Microscopic pictures of the failed 1200 V IGBT chips during surge-current at V_{GE} = 40 V with (a) 1EB and (b) 3EB.

1200 V IGBT			
V_{GE}	Emitter bond wire type	Last-pass surge-current density	I^2t
25 V	1EB	3.10 a.u.	9.25 a.u.
	3EB	3.15 a.u.	9.35 a.u.
40 V	1EB	3.80 a.u.	13.60 a.u.
	3EB	4.40 a.u.	17.50 a.u.

Table 1: Comparison of the last-pass surge-current capability of the 1200 V IGBT at different V_{GE} for 1EB and 3 EB.

Further, the impact of the number of emitter bond wires on surge-current capability was studied for 650 V and 1700 V IGBTs. For this, selected emitter bond wires were cut to reduce the number of bond wires. The 650 V IGBT consists of two segmented emitter pads and each pad has two bond wires. As shown in Fig. 11, for case-1 a single bond wire from each pad was cut and two bond wires from the same emitter segment were cut for case-2. The 1700 V rated IGBT consists of four segmented emitter pads and each pad has three bond wire connections. Here, for case-1, two bond wires were cut, which leads to 33% reduction in the effective wire diameter for the chip and 66% reduction for case-2 as shown in Fig. 14.

(a) (b)

Fig. 11: Surge-current measurements with cut emitter bond wires for 650 V IGBT (a) a single bond wire was cut from each pad (b) two bond wires were cut from same emitter segment.

For case-1 (650 V) the measured $V_{CE,load}$ is plotted for the increased surge-current amplitude in Fig. 12(a). Here, the pristine devices refer to IGBTs without any emitter bond wire cut. At V_{GE} = 25 V, the surge-current capacity is reduced by 18% as compared to the pristine device [Fig. 2(b)] for the same measurement condition. This is because of the higher current density. Further, the surge-current capability is drastically reduced by 60% for case-2, see Fig. 12(b). In this case, all the current has to flow via the single emitter pad with two emitter bond wires. According to measurements and failed pictures, the destruction threshold is not determined by the onset of intrinsic conductivity. Due to the limited robustness of the front side contact against excessive heat, the failure signature indicates a temperature-driven destruction mechanism [11]. As shown in Fig. 13, the Al pad near the bonding wire has experienced thermal fatigue [16]. The last-pass surge-current and I^2t of the 650 V IGBT at different cases is summarized in the Table 2.

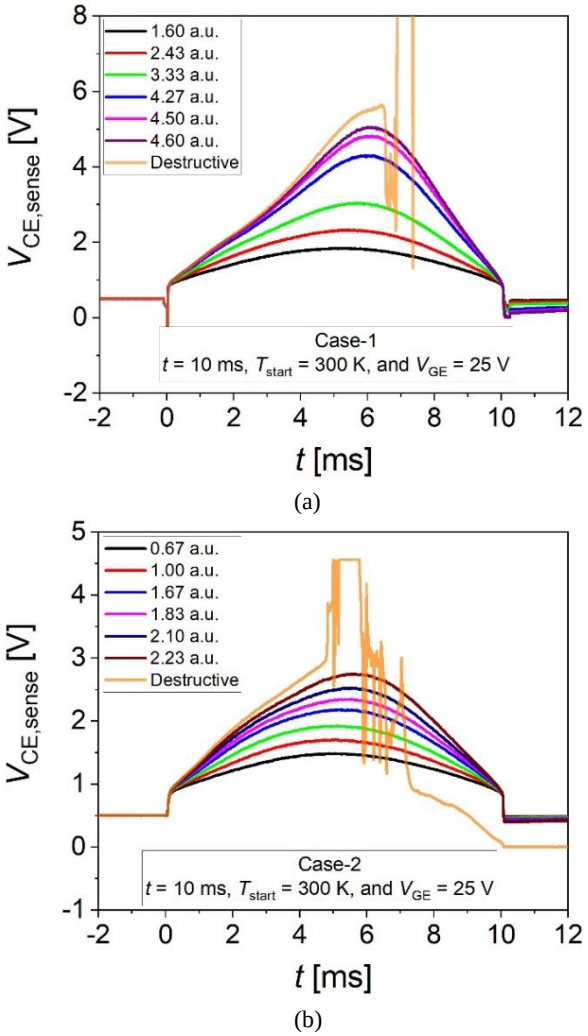

(a)

(b)

Fig. 12: Measured $V_{CE,load}$ across the 650 V IGBT for increasing the surge-current density amplitude at V_{GE} = 25 V with reduced emitter bond wires (a) case-1 (b) case-2. For a given condition of t_p = 10 ms, and T_{start} = 300 K.

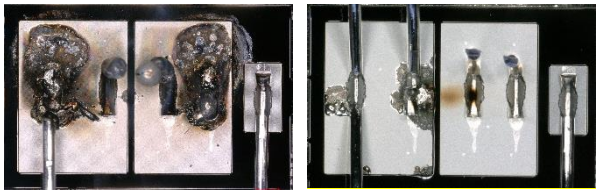

(a) case-1 (b) case-2

Fig. 13: Microscopic pictures of the failed 650 V IGBT chips during surge-current at V_{GE} = 25 V with reduced bond wires (a) a single bond wire was cut from each pad (b) two bond wires were cut from same emitter segment.

650 V IGBT			
V_{GE}	**Emitter bond wire type**	**Last-pass surge-current density**	I^2t
25 V	Pristine	5.63 a.u.	28.80 a.u.
	case-1	4.60 a.u.	17.50 a.u.
	case-2	2.23 a.u.	4.50 a.u.

Table 2: Comparison of the last-pass surge-current capability of the 650 V IGBT at different cases.

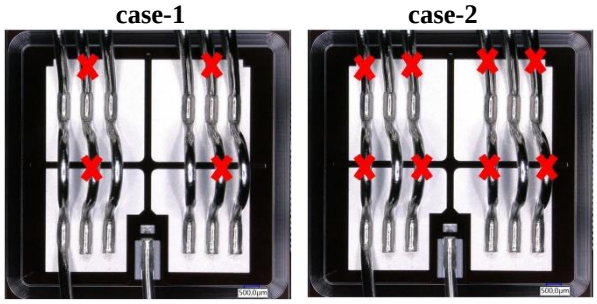

(a) (b)

Fig. 14: Surge-current measurements with cut emitter bond wires for 1700 V IGBT (a) 33% reduction in effective emitter bond wire diameters (b) 66% reduction.

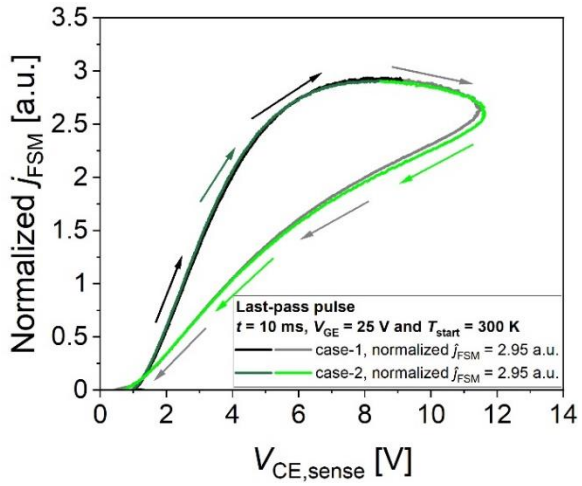

Fig. 15: Measured last-pass normalized surge-current pulse of 1700 V chip on DCB IGBT at V_{GE} = 25 V for case-1: 33% reduction and case-2: 66% reduction. Given conditions: t_p = 10 ms, and T_{start} = 300 K.

For 1700 V IGBT bond wire modification, the impact is not significant. For both cases, a similar surge-current robustness at V_{GE} = 25 V is achieved. There is a slight 3% reduction in the last-pass surge-current as compared to the pristine 1700 V device capability [Fig. 3(b)]. As can be seen from Fig. 15, the IGBT with 66% reduced bond wires shows slightly higher $V_{CE,sense}$ drop as compared to the IGBT with 33% reduction for the same current density. This can be due to the increased resistance of bond wires in combination with higher temperatures. The failure occurs around the bond wires as shown in Fig. 16. The failure signature becomes stronger with less number of emitter bond wires.

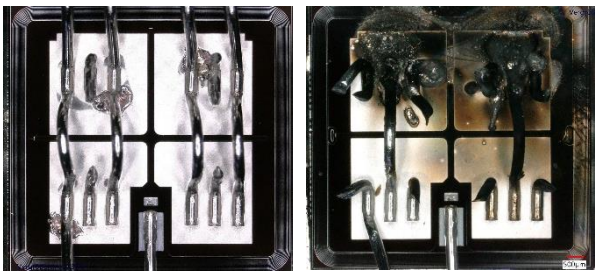

(a) case-1 (b) case-2

Fig. 16: Microscopic pictures of the failed 1700 V IGBT chips during surge-current at V_{GE} = 25 V with (a) 33% reduction in effective emitter bond wire diameters (b) 66% reduction.

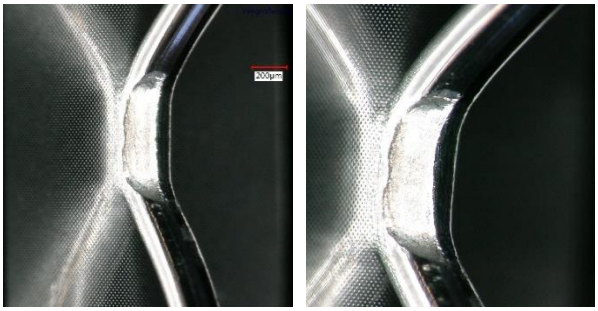

(a) Before surge-current (b) Last-pass pulse

Fig. 17: Microscopic pictures of an 1EB IGBT(a) Before surge-current pulse and (b) Last-pass pulse with $\hat{j}_{FSM}$ = 310 a.u. Conditions: t_p = 10 ms, and T_{start} = 300 K.

For all different voltage class IGBTs, microscopic images were recorded during the intermediate single pulse surge-current event to study a possible change in Al metallization with a special focus on the bond foot areas. However, there was no distinguishing difference observed on the Al metallization surface between the new device and the same device before reaching the last-pass event. An IGBT with 1EB is displayed in Fig. 17 with a focus around the bond wire wedges area before the surge-current event and after the last-pass pulse.

CONCLUSION

The surge-current behaviour of IGBTs with different rated blocking voltages has been analysed in detail by measurements. For a fixed gate-emitter voltage, the surge-current capability of the IGBT is limited due to the channel pinch-off. For a V_{GE} of 25 V, the tested devices could withstand up to 6 ... 7 times the rated current at starting temperature of 300 K and 5 ... 6 times at 425 K,

respectively. The 650 V IGBT withstands a higher surge-current density as compared to 1200 V and 1700 V IGBTs. However, at V_{GE} of 25 V and 300 K, the 650 V last-pass surge-current density is noticeably reduced compared to its saturation current in the output characteristic at room temperature. For shorter surge-current pulse duration, a higher surge-current can be withstood. For that, the thermal impedance (Z_{th}) of the respective chip and interconnection technology in combination with the self-heating plays an important role.

The number of emitter bond wires does not show any influence on the surge-current capability of 1200 V and 1700 V devices up to gate-emitter voltages of 25 V. For V_{GE} = 40 V, the 1200 V device shows a surge-current capability difference of 16% between 1EB and 3EB IGBTs. On the other hand, the 650 V IGBTs surge-current capability is influenced by the number of bond wires already at 25 V due to its higher saturation current density.

For all the measured conditions, the different voltage class IGBTs fail due to strong V_{CE} desaturation. This confirms our initial statement that there is a trade-off relationship regarding the IGBT's surge-current capability and it's short-circuit capability.

REFERENCES

[1] T. Basler, J. Lutz, R. Jakob, et. al, "Surge Current Capability of IGBTs", in Proc. of 9th International Multi-Conference on Systems, Signals and Devices, pp. 1-6, 2012.

[2] T. Basler, J. Lutz, R. Jakob, "IGBTs Conducting Diode-Like Surge Currents", in Proc. of 26th ISPSD, pp. 103-106, Hawaii, USA, June 15-19, 2014.

[3] J. Kowalsky, T. Simon, M. Geske, et. al, "Surge Current Behaviour of Different IGBT Designs", in PCIM Europe, pp. 502-511, Nuremberg, May 19-21, 2015.

[4] T. Basler "Ruggedness of high-voltage IGBTs and Protection Solutions", universitätsverlag, Chemnitz, 2014.

[5] J. Lutz, H. Schlangenotto, U. Scheuermann, R. De Doncker, "Semiconductor Power Devices: Physics, Characteristics, Semiconductor Power Devices: Physics, Characteristics, Reliability," 2nd ed. Berlin, Germany: Springer-Verlag, 2018.

[6] S. Yin, Y. Gu, S. Deng, et al, "Comparative Investigation of the Surge Current Capabilities of Si IGBT and SiC MOSFET for Pulsed Power Application", in IEEE transactions on Plasma Science Vol. 46, No. 8, August 2018.

[7] F. Schork, R. Brocke, M. Rock, et al, "Surge current capability of power electronics for surge protection", in PCIM Asia 2016, Shanghai, China, 28 – 30 June 2016.

[8] D. Silber, M. J. Robertson, "Thermal effects on the forward characteristics of silicon p-i-n diodes at high pulse currents" in Solid-State Electronics, 16(12), 1973

[9] A. P. Silard; "High-temperature physical effects underlying the failure mechanism in thyristors under surge conditions" in IEEE Transactions on Electron Devices, 31(9), 1984

[10] R. Baburske, T. Basler, J. Lutz, H.-J. Schulze et al. "The Trade-Off between Surge-Current Capability and Reverse-Recovery Behaviour of High-Voltage Power Diodes" in 10th International Seminar on Power Semiconductors (ISPS); 2010

[11] T. Hunger, O. Schilling, F. Wolter, "Numerical and experimental study on surge current limitations of wire-bonded power diodes", in PCIM Europe, Nuremberg, May, 2007.

[12] Z. Li, G. Zeng, J. Kowalsky, et al, "Investigation on the interaction between surge current pulses and power cycling test", in Proc. of ISPS, Prague, Czech Republic, 2018.

[13] S. Palanisamy, J. Kowalsky, J. Lutz, et al, "Repetitive surge current test of SiC MPS diode with load in bipolar regime", in Proc. of 30th ISPSD, pp. 367-370, Chicago, USA, May 13-17, 2018.

[14] A. Baschnagel, U. Schlapbach, "Surge currents for IGBT diodes", Application notes, ABB Switzerland Ltd, Lenzburg, Switzerland.

[15] M. Ke, D. Li, X. Dai, et al, "Improved Surge Current capability of Power Diode with Copper Metallization and Heavy Copper Wire Bonding", in 18th EPE'16 ECCE Europe, Karlsruhe, Germany, Sep. 05 - 09, 2016.

[16] W. Zhong, Y. Tang, C. Li, et al, "Electro-thermal Analysis of 1.2kV – 100A SiC JBS Diodes Under Surge Current Stress", in 16th SSLChina: IFWS, Shenzhen, China, Nov. 25 - 27, 2019.

Addresses of the authors

Madhu Lakshman Mysore, Reichenhainer Str. 70, Chemnitz, Germany, madhu-lakshman.mysore@etit.tu-chemnitz.de
Mohamed Alaluss, Reichenhainer Str. 70, Chemnitz, Germany, mohamed.alaluss@etit.tu-chemnitz.de
Felix Fraas, Einsteinstraße 12, Unterschleißheim, Germany, felix.fraas@wolfspeed.com
Thomas Basler, Reichenhainer Str. 70, Chemnitz, Germany, thomas.basler@etit.tu-chemnitz.de
Josef Lutz, Reichenhainer Str. 70, Chemnitz, Germany, josef.lutz@etit.tu-chemnitz.de
Roman Baburske, Infineon Technologies AG, Neubiberg, Germany, roman.baburske@infineon.com
Franz-Josef Niedernostheide, Infineon Technologies AG, Neubiberg, Germany, franz-josef.niedernostheide@infineon.com
Hans-Joachim Schulze, Infineon Technologies AG, Neubiberg, Germany, schulze.external9@infineon.com